AIChE

Rheological Characterization of Olivine Slurries, Sheared Under CO_2 Pressure

Fabien Mahaut,[a] Georges Gauthier,[a] Philippe Gouze,[b] Linda Luquot,[b] Dominique Salin,[a] and Jérôme Martin[a]

[a]FAST, CNRS UMR 7608, Université Paris Sud - 11, bât. 502 Campus Universitaire 91405 Orsay cedex, France; martin@fast.u-psud.fr (for correspondence)

[b]Géosciences Montpellier, CNRS UMR 5243, Université Montpellier 2, 34095 Montpellier cedex 5, France

Published online 5 August 2013 in Wiley Online Library (wileyonlinelibrary.com). DOI 10.1002/ep.11826

The injection of reactive mineral suspensions is a possible process to either reinforce or seal wells in geologic carbon sequestration sites. Among others, olivine slurries could be used as CO_2-triggered cements, as they carbonate under the thermodynamic conditions of deep storage. However, injection of such slurries requires to control their initial fluidity and its evolution during the displacement. For this purpose, we have characterized the rheological evolution of olivine suspensions, of particle sizes 1−10 μm, sheared at 100 s^{-1}, in the ranges of 10−40% for the volume fractions, 20−50 bars for the CO_2 pressure, and 60–110°C for the temperature. The apparent viscosity, measured at 100 s^{-1}, increases exponentially, with a characteristic time ranging from less than 1 h to more than 10 h, and decreasing with olivine concentration, CO_2 pressure, and temperature. Moreover, a careful characterization of the slurry rheology carried out in the initial stages of slow evolution, shows that the slurry obeys a Bingham plastic law, with a yield stress Σ_B, and a Bingham viscosity μ_B increasing from 1 to 20 Pa and from 4 to 110 mPa s, respectively, when the olivine volume fraction φ is increased from 10 to 30%. Such variations can be accounted by classical models (Wildemuth and Williams [1984]: Rheologica Acta, 23,627–635, Krieger [1972]: Advances in Colloid and Interface Science, 3, 111–136).

Keywords: carbon sequestration, mineral carbonation, slurry injection, well remediation, Bingham plastic

INTRODUCTION

One of the main concern regarding CO_2 geological sequestration is the risk of leakage through fractures in either the caprock or the plugged injection wells. Fracturing due to mechanical or chemical stresses may be triggered by natural events (e.g., tectonics) but also by the well completion or the CO_2 injection. For a leaky well, the prevailing strategy, inherited from oil industry, is to fill the well with viscous (heavy) slurries and/or concrete. If the leakage issues from the alteration of the cements or the caprock around the well (outside the steel tubing), then cement is locally injected. But although complex and costly, such remediation may not be fully satisfactory. As the injected cement can hardly penetrate deeply in porous media or in small aperture rough fractures, the interface between the sealing cement and the leaky material may remain mechanically weak. Furthermore, *albeit* portland-type cements are considered as poorly reactive with CO_2, some recent experiments [1] indicate that they may react when exposed to flowing CO_2-rich fluid. Accordingly, the use of such cements for sealing issues is questionable. Good alternative candidates could be light slurries (suspensions) composed of magnesium silicate minerals (e.g., olivine or serpentine).

Such minerals were investigated by O'Connor *et al.* [2] for ex situ carbonation/uptake of CO_2, as their carbonation, at high temperature and under high CO_2 pressure, enables mineral carbon dioxide sequestration. And as the carbonation of olivine (forsterite Mg_2SiO_4) leads to the formation of magnesite ($MgCO_3$), with an increase of the solid phase volume which can reach 88% [3], O'Connor *et al.* [4] suggested that olivine slurries could also be used for in situ preventive reinforcement of wells. Such a technique would present several advantages: olivine and serpentine are present worldwide in greenstone belts and ophiolites, ultramafic rocks grinding is already used in industrial applications (refractory cements, light blasting, abrasives, etc.). Moreover, as a candidate for CO_2 sequestration process, the dissolution/carbonation of olivine and serpentine is already well documented [5–7] and although such a carbonation process may be too expensive for mineral sequestration purposes, it could lead to a rather cheap and efficient process for either preventive well reinforcement or sealing issues. However, the technique is still speculative because of the lack of experimental data.

The present work aims at characterizing the rheometric properties of olivine slurries, and their time evolution. We first present measurements of the apparent viscosity of sheared (at 100 s^{-1}) aging olivine slurries. The olivine volume fraction is varied in the range 10−40%, the CO_2 pressure in the range 20−50 bars, and the temperature in the range 60–110°C. These tests show that a time laps exists, during which the olivine slurries keep a rather low apparent viscosity which should allow injection. The rheologic properties of the slurries at this early stage are then further characterized by their stress response to different shear

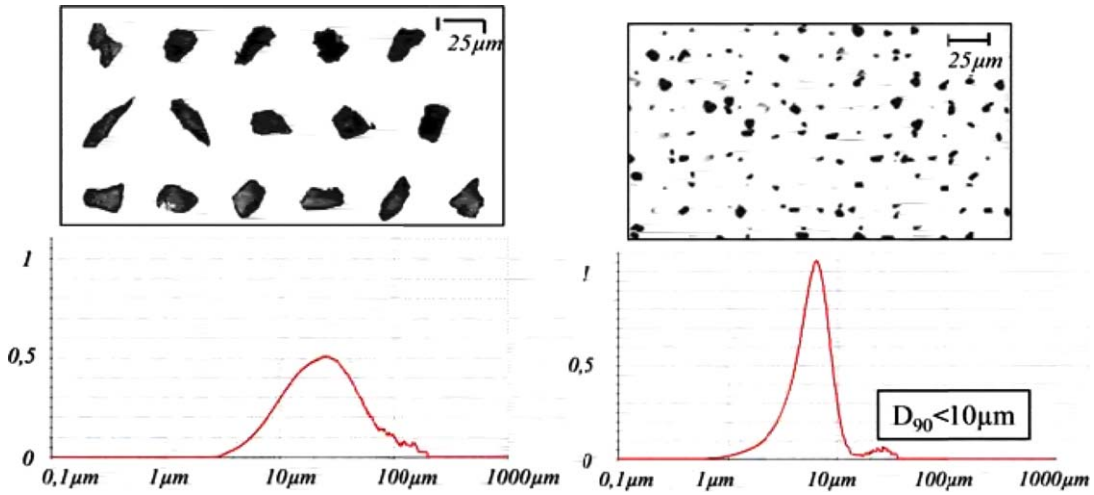

Figure 1. Size distribution and snapshots of the olivine particles, before (left) and after (right) micronization. [Color figure can be viewed in the online issue, which is available at **wileyonlinelibrary.com**.]

rates. The olivine slurry is shown to obey a non-Newtonian Bingham equation. The corresponding yield stress and Bingham viscosity both increase with the olivine volume fraction, in accordance with models found in the literature [8,9].

OLIVINE SLURRIES AND EXPERIMENTAL DEVICES

Olivine Suspensions

Olivine suspensions were prepared with Volvic mineral water and olivine particles, of chemical composition $Mg_{1.8}Fe_{0.2}SiO_4$ (with traces of iron sulfate $FeSO_4$, diopside $CaMgSi_2O_6$, and spinel $MgAl_2O_4$) provided by Micronizzati MS. However, the initial particle size distribution was rather high (Figure 1, left), with most of the particles in the range 10–100 µm ($D_{90} \approx 100$ µm, i.e., 90% of the particles have a diameter smaller than 100 µm), and their sedimentation rate was too high to conduct rheological characterization, and to expect the suspensions to be injectable. To cope with this problem, the particle size was first decreased to $D_{90} \approx 10$ µm (Figure 1, right), using air flow micronization in a spiral jet mill, which did not change the chemical composition. With such a size reduction, the typical Stokes velocity was about 130 µm s^{-1} for an olivine particle of density 3.36 g cm^{-3}, and of typical diameter 5 µm. The slurries prepared at various olivine fractions φ, were found to be fluid at $\varphi < 30\%$, and very pasty at higher concentrations. Therefore, we focused our studies on suspensions at $\varphi < 30\%$, which were easier to handle and which were more likely to be injectable.

Rheometer Setup

To characterize the evolution of rheological properties, at fixed temperature and CO_2 pressure, we used an Anton Paar MCR501, equipped with a High Pressure (HP) cell. This commercial HP cell enables rheological tests at pressures up to 150 bars and controlled temperatures up to 300°C, but has some drawbacks.

First, the HP cell has only one geometry (Couette concentric cylinders, of inner and outer radii $R_i = 12.5$ mm and $R_e = 13.5$ mm, over a height $h = 36$ mm), and the bob has a conical extremity whereas the cup has a plane bottom. As a consequence, the volume between the cup bottom and the bob extremity is submitted to a shear rate significantly lower than the shear rate imposed in the gap of the cell. As a result, both shear-induced diffusion [10] and sedimentation drive the particles toward the bottom of the cell. The suspension may become nonuniform, leading to erroneous rheological measurements and time characterization. To prevent such nonuniformity, we have used a designed in-house cup, with a conical bottom (Figure 2). The resulting geometry ensures an almost homogeneous shear rate in the whole volume of sheared suspension, and prevents the migration of particles [11]. The second drawback of the HP cell is due to its magnetic coupling which decreases the accessible range of the rheometric measurements. Whereas

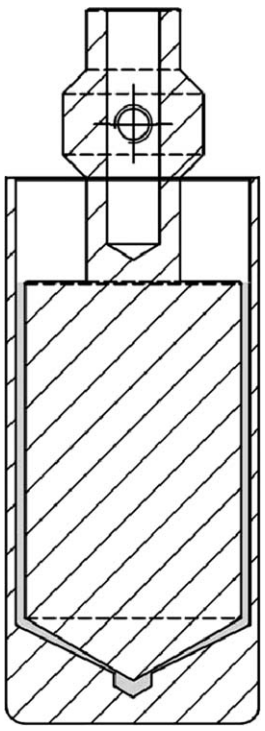

Figure 2. Geometry of the rheometer cell. The conical bottom of the cell ensures an almost homogeneous shear rate in the whole volume of sheared suspension

the minimum torque is equal to 0.01 μN m in classical cells, it is increased to 100 μN m in the HP cell, which corresponds to a shear stress of about 3 Pa, and, for a typical shear rate of 100 s^{-1}, to a minimum measurable viscosity of about 30 mPa s.

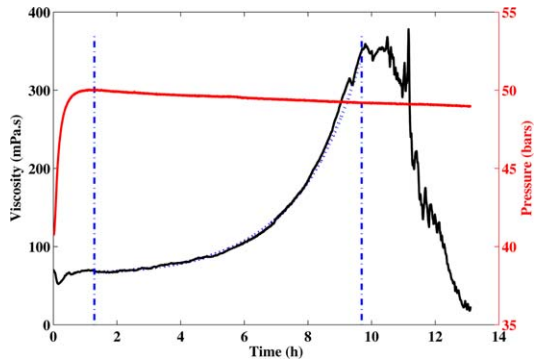

Figure 3. Typical evolution of the apparent viscosity (black curve, left axis) and pressure (red curve, right axis), obtained for an olivine suspension at volume fraction $\varphi = 20\%$, at $\dot{\gamma} = 100\ s^{-1}$, $T = 80°C$, and $P_{CO_2} = 40$ bars. The two vertical dash-dotted lines delineate three successive stages: An initial stage, corresponding to the onset of the pressure and temperature, a second stage of exponential increase of the apparent viscosity, and a third stage of noisy decrease of the viscosity measurement. The blue dotted line displays an exponential fit, with a characteristic time $\tau = 2$ h. [Color figure can be viewed in the online issue, which is available at **wileyonlinelibrary.com**.]

Rheological Characterization

Evolution of Apparent Viscosity: Aging of Sheared Suspensions

To address the aging time scales and the fluidity evolution of the olivine suspensions, we first monitored the apparent viscosity, measured at the constant shear rate $\dot{\gamma} = 100\ s^{-1}$, for different olivine concentrations and thermodynamic conditions.

Note that the value of the shear rate has been selected to ensure an efficient stirring and a measurable viscosity value, for olivine suspensions of typical volume fraction 15–20%. The experimental procedure is the following: A volume of

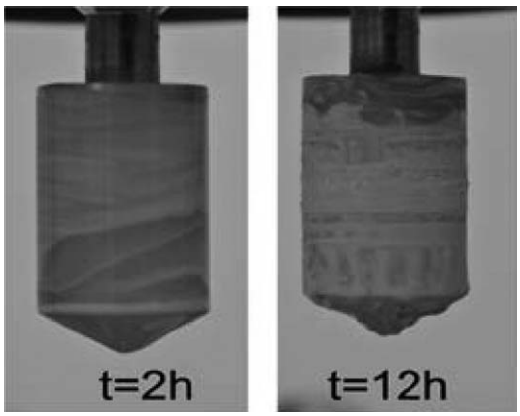

Figure 4. Snapshots of the rotor at $t = 2$ h and 12 h, for the experimental parameters of Figure 3.

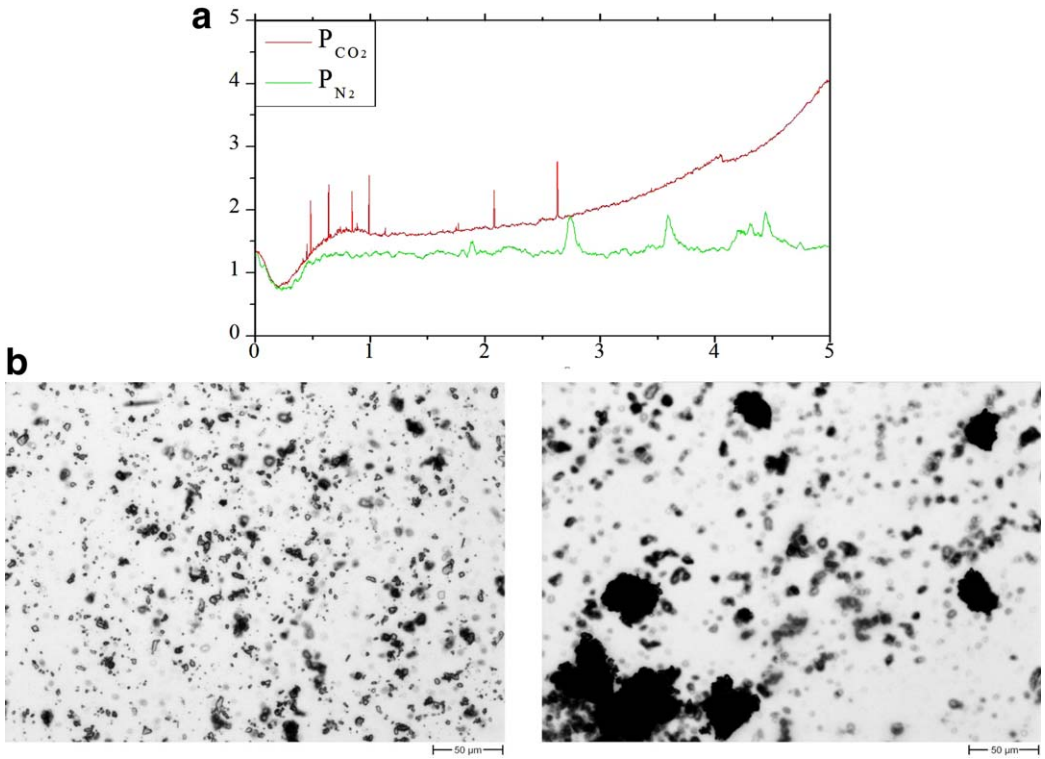

Figure 5. Comparison of the apparent viscosity recorded under pressure of nitrogen or carbon dioxide (top), and snapshots of the resulting suspensions (bottom), obtained for tests at volume fraction $\varphi = 20\%$, $\dot{\gamma} = 100\ s^{-1}$, $T = 100°C$, and $P_{N_2} = 40$ bars (left) and $P_{CO_2} = 40$ bars (right), respectively. [Color figure can be viewed in the online issue, which is available at **wileyonlinelibrary.com**.]

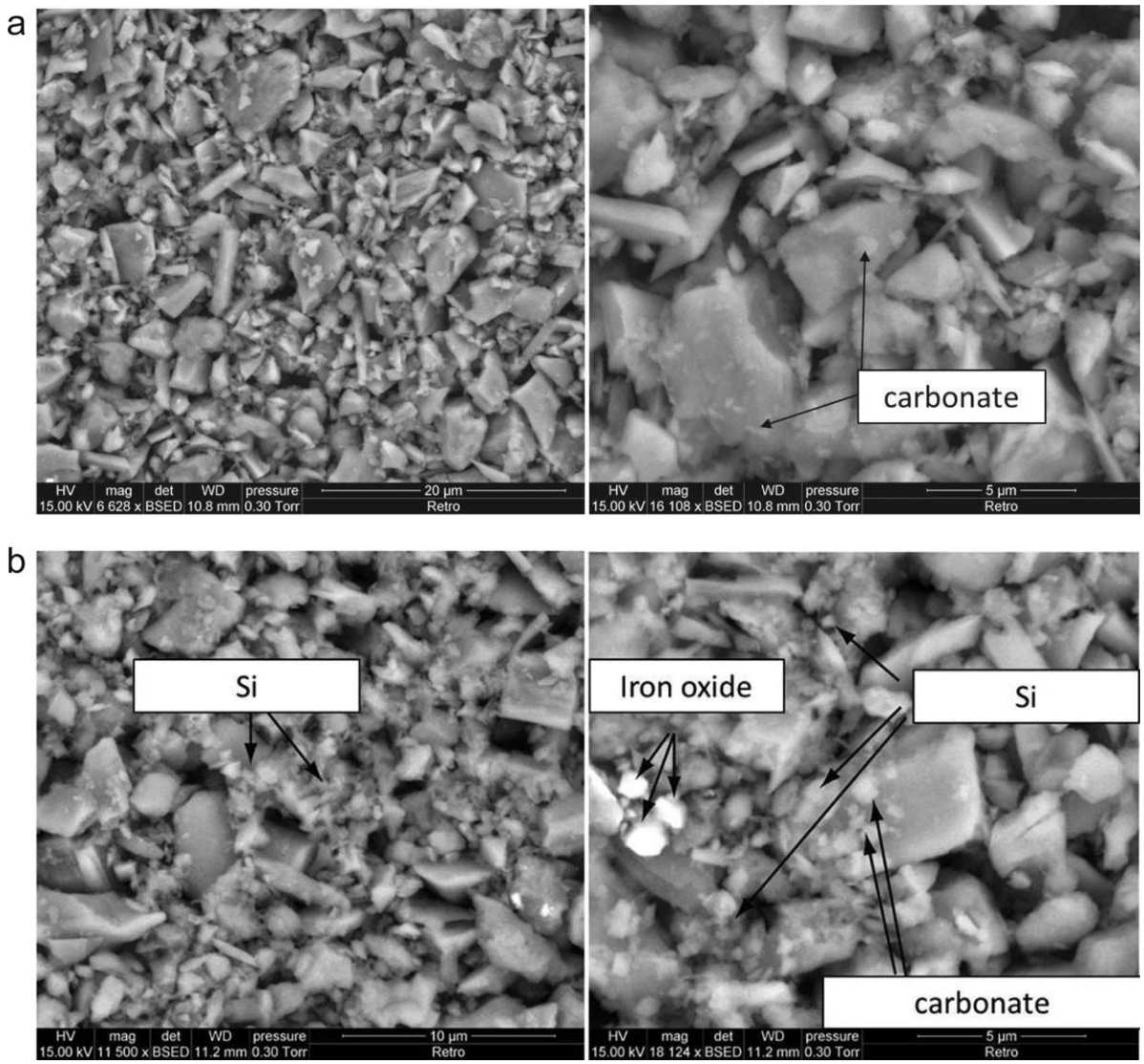

Figure 6. Scanning Electron Microscope (SEM) images of the particles after 7 h (top) and 13 h (bottom) for a slurry at volume fraction $\varphi = 20\%$, sheared at $\dot{\gamma} = 100\ s^{-1}$, at $T = 80°C$, and $P_{CO_2} = 40$ bars.

3 cm^3 of freshly mixed olivine suspension is introduced in the HP cell, at room temperature $T_r = 20°C$. The cell is closed, connected to carbon dioxide at pressure P_{CO_2}, bleeded, and connected again. The cell is then isolated and heated up to the set point temperature T, which results in an increase of the pressure in the cell (in the expected ratio $T(K)/T_r(K)$, where $T(K)$ is the temperature in Kelvin), whereas the apparent viscosity measured at constant shear rate, is recorded.

A typical record of the apparent viscosity, obtained for an olivine suspension at volume fraction $\varphi = 20\%$, at $\dot{\gamma} = 100\ s^{-1}$, $T = 80°C$, and $P_{CO_2} = 40$ bars, is displayed in Figure 3. Three stages may be identified. The first one has a duration of about 1 h. It corresponds to the initial onset of a uniform temperature T inside the cell. It is accompanied by a corresponding increase of the CO_2 pressure, and ends with initial plateau values for both the pressure and the measured viscosity. The second stage, of variable duration (about 8 h in the displayed example), corresponds to an increase of the apparent viscosity, which can be fitted by an exponential growth (dotted blue line). The third stage corresponds to a very noisy decrease of the viscosity measurement, down to unmeasurable values. This unexpected decrease of the viscosity may be enlightened by the comparison of the slurry state in the early second stage (at time $t = 2$ h), and at the end of the third one ($t = 12$ h), for the parameters of Figure 3.

At $t = 2$ h, the slurry is found in a homogeneous state very similar to the initial one, which is a rather fluid state for suspensions at $\varphi = 20\%$. When the bob is removed from the cell, the fluid slurry flows down, and leaves a thin layer of suspension (left snapshot of Figure 4). On the opposite, when the cell is opened at $t = 12$ h, two phases can be identified: A water-like supernatant liquid phase, and a very thick pasty phase, which sticks to the surfaces of the cup and the bob. When the bob is removed from the cell, the slurry does not flow at all, and stays in a thick solid layer on the bob surface (right snapshot of Figure 4). It is conceivable then that the third stage of the apparent viscosity record corresponds to the fracturing of the thickening slurry, which generates noise in the rheogram, and results in the localization of the shear in a layer of suspending fluid (shear banding effect). However, such an effect may be seen as an artefact of our rheological test, in which a constant shear rate is imposed on a setting slurry, with no limitation of the required stress. In practical applications, the pressure head is

fixed (or at least limited), and the phenomena observed during the third stage are likely to be irrelevant: the thickening of the slurry toward a solid state would result in clogging, rather than in an apparent conductivity increase, that one could naively expect from the decrease of the measured viscosity. For these reasons, we focus in the following on the second phase, which is indeed more relevant to address injection issues.

To get some insight into the cause of the thickening, the records of the apparent viscosity, under carbon dioxide and under nitrogen are compared in Figure 5. In the absence of CO_2, no thickening of the olivine slurry is observed, during a 5 h long test: It has been suppressed, or at least delayed. Moreover, the comparison of the suspensions (bottom photographs of Figure 5) reveals that in the suspensions aging under CO_2 pressure, the particles form clusters, which is expected to result in the thickening of the suspensions [12]. These observations lend credit to the formation of clusters of olivine particles, stuck by the olivine dissolution-carbonation reaction:

$$Mg_2SiO_4 + 2CO_2 \rightarrow 2MgCO_3 + SiO_2. \quad (1)$$

Such a reaction is substantiated by local chemical analysis using a Scanning Electron Microscope (SEM) of the solid phase after 7 and 13 h of aging process (Figure 6). First, the size observed for the initial particles, and for the 7 and 13 h old suspensions, is smaller and smaller, which supports some acid dissolution of the olivine. Second, the products of the olivine dissolution-carbonation reaction, namely phases rich in carbonate, iron oxide and silicon (which could be either silica or amorphous silicon) are present after aging under CO_2 as observed by Andreani *et al.* [3].

To characterize the kinetics of the rheological evolution of the olivine slurries, the influence of the different parameters on the evolution of the apparent viscosity has been studied and quantified by the estimation of the characteristic time τ of the exponential increase of viscosity during the second stage. Figure 7 displays the curves obtained at temperatures between 60 and 110°C, at $\varphi = 20\%$, $\dot{\gamma} = 100\ s^{-1}$, $P_{CO_2} =$ 40 bars. A strong decrease of τ (from 14 to 2 h) is observed when the temperature is increased from 60 to 80°C, whereas τ hardly changes (i.e., τ remains at a value close to our time resolution) when the temperature is further increased. It is likely that τ is controlled by the dissolution rate r of the olivine, which obeys an Arrhenius law $r \propto \exp(-E_a/RT)$. Indeed, the semi-log plot of the variations of $\tau \propto 1/r$ with $1/T(K)$ (inset of the bottom Figure 7) is rather linear. Moreover, the corresponding slope E_a/R gives $E_a = 66.2$ kJ mol^{-1}, comparable with the value $E_a = 66.5$ kJ mol^{-1} obtained by Jonckbloedt [13] in acidic solutions. We note however that such a good agreement may be rather fortuitous, as E_a has been reported to vary from 38 to 126 kJ mol^{-1}, depending on the experimental conditions [14]. The different values of τ, obtained for CO_2 pressures fixed between 20 and 52 bars, at $\varphi = 20\%$, $\dot{\gamma} = 100\ s^{-1}$, $T = 90$°C, are displayed in Figure 8. Although the experiments display some variability, a decrease of P_{CO_2} is clearly associated with a delay of the apparent viscosity increase. This trend is illustrated in the graph $\tau(P_{CO_2})$: The characteristic time is decreased by a factor of about five when the CO_2 pressure is increased from 20 to 50 bars. The data are also displayed in log–log scale (inset of the bottom Figure 8) to test a power law behavior. The best fit has an exponent of 2.15, but it is unclear if the slope remains constant or increases from ~2 at low P_{CO_2} to ~0.5 at high P_{CO_2}. Actually, the solution in our experiments is expected to be mildly acid (mineral water at pH = 7, under CO_2 pressure), and the kinetics of the dissolution of the olivine, in this range of experimental conditions, may be rather

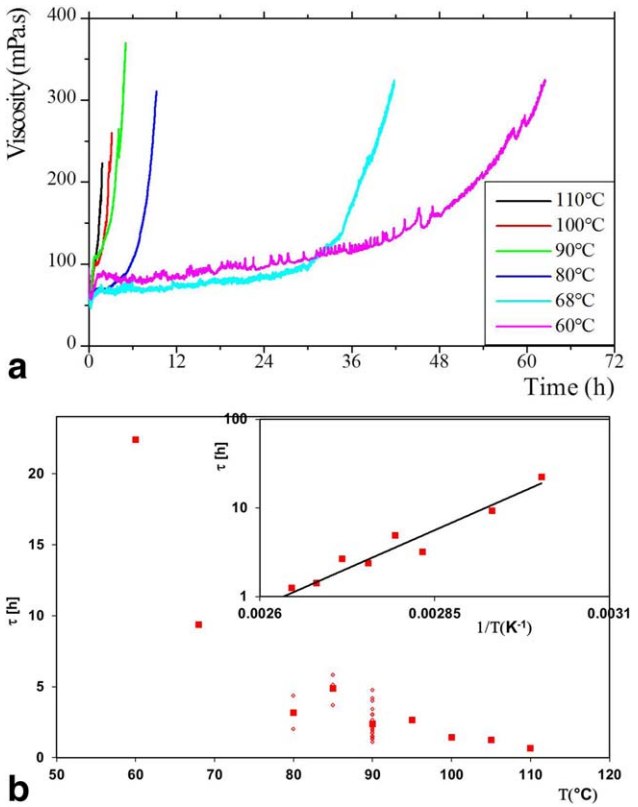

Figure 7. Comparison of the apparent viscosities recorded at different temperatures (top) and the corresponding characteristic times τ (bottom), obtained for tests at volume fraction $\varphi = 20\%$, $\dot{\gamma} = 100\ s^{-1}$, $P_{CO_2} = 40$ bars. The open diamonds are one run data, whereas the filled squares are averaged measurements. The inset diagram is a semi-log plot of τ versus $1/T(K)$, with an Arrhenius fit to the averaged data (straight line). [Color figure can be viewed in the online issue, which is available at **wileyonlinelibrary.com**.]

complex: The order of the pH dependence may change around pH = 5 [14] or pH = 7 [15], and depends also on the concentrations of the other ions [15,16]. Besides, we note that the smaller estimated values of the characteristic times ($\tau \sim 1.5$ h) are the lower values accessible in our experiments: They correspond to a continuous transition between the onset of the experimental conditions of temperature and pressure (first stage) and the divergence of the measured apparent viscosity (third stage). The measurement of shorter times τ, expected for higher pressures P_{CO_2}, are thus beyond the time resolution of our experimental protocol. Thence, our data on the effect of P_{CO_2} on the rheological aging of a flowing slurry remain partly inconclusive. Further understanding would require to enlighten our data, obtained under controlled flow conditions, with data obtained under controlled chemical conditions (with the monitoring of the pH and chemical concentrations).

To complete the aging issue, the apparent viscosities recorded for different concentrations of olivine ($15\% < \varphi < 30\%$) are displayed in Figure 9. A significative delay of the slurry evolution is observed when the concentration is decreased down to $\varphi = 15\%$. Conversely, τ vanishes for initial concentrations of olivine higher than 30% (bottom graph of Figure 9). In this range ($30\% < \varphi < 40\%$), the initial slurries were pasty, and it was actually difficult to fill the cell, because they did not flow out of the vessel. This

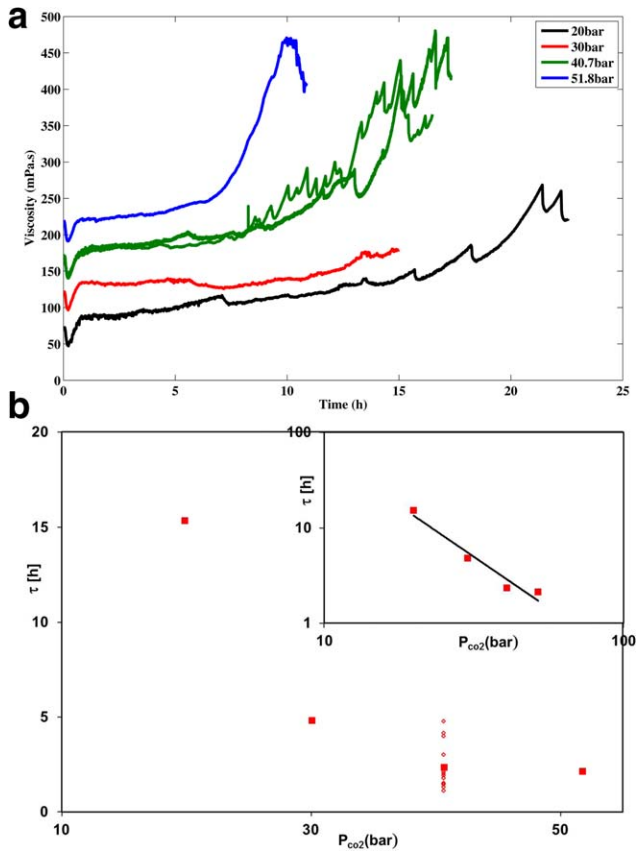

Figure 8. Comparison of the apparent viscosities recorded under various pressures of CO_2 (top, displayed with an arbitrary shift), and the corresponding characteristic times τ (bottom), obtained for tests at volume fraction $\varphi = 20\%$, $\dot{\gamma} = 100$ s^{-1}, $T = 90°C$. The open diamonds are one run data, whereas the filled squares are averaged measurements. The inset displays the average data in log–log scales. [Color figure can be viewed in the online issue, which is available at **wileyonlinelibrary.com**.]

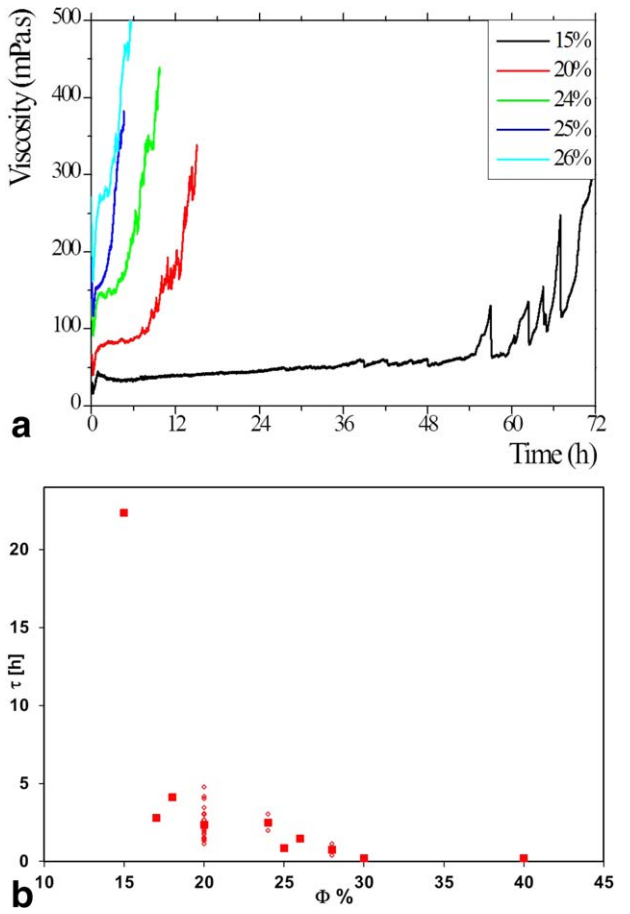

Figure 9. Comparison of the apparent viscosities recorded at different olivine concentrations (top) and the corresponding characteristic times τ (bottom), obtained for tests at $\dot{\gamma} = 100$ s^{-1}, $T = 90°C$, $P_{CO_2} = 40$ bars. [Color figure can be viewed in the online issue, which is available at **wileyonlinelibrary.com**.]

suggests that these slurries have a yield stress, under which they would not flow. This property cannot be evaluated with an apparent viscosity record, and requires a more complex rheological characterization, such as stress–strain curves discussed in the following.

Bingham Plastic Characterization

To address the issue of the non-Newtonian behavior of the olivine slurries, some rheological tests have been carried out, as the response to either steps in shear rate or steps in shear stress. These tests require a time window, during which the system will not evolve significantly. Thence, they have to be applied during the plateau of the second stage (Figure 3), in slurries aging with a large enough characteristic time τ. Both steps in shear rate or in shear stress have been tested. However in the latter case, the system was difficult to control: The rheometer rotation was stopped at low enough applied stress, whereas a very high shear rate was obtained for stresses above some value. Such a response evidences the existence of a yield stress. We note also that it was associated with important hysteresis, probably due to strong modifications of the slurry state in the absence of stirring. To circumvent this drawback, the non-Newtonian behavior of the olivine slurries was investigated through the response to shear rate steps.

The top panel of Figure 10 displays the apparent viscosity measured on an olivine slurry, at $\varphi = 20\%$, $\dot{\gamma} = 100$ s^{-1}, $T = 90°C$, which was submitted to shear rate steps every 2 h (apparent viscosity in red symbols), and continuously sheared at $\dot{\gamma} = 100$ s^{-1} in the mean time (apparent viscosity in black symbols). First, the record of the apparent viscosity at $\dot{\gamma} = 100$ s^{-1} compares very nicely with the one obtained for similar parameters, and without shear steps, displayed in Figure 3, during the first 6 h. However, at $t = 6$ h, the response to the third shear steps sequence is followed by a discontinuity of the apparent viscosity, which becomes more noisy thereafter (probably due to the appearance of some shear banding phenomena). And we note that the subsequent shear steps sequences display also some hysteresis (i.e., discontinuity of the apparent viscosity). For the above reasons, we will focus in the following on the response to the first sequence, at $t = 2$ h, as it does not alter the aging process, and it applies to a "quasi-static" state of the slurry. This shear rate steps sequence consisted in three 100 s long steps at $\dot{\gamma} = 50$, 150, 200 s^{-1} (blue dotted line, right axis, in the inset of Figure 10). The corresponding response in shear stress (open red squares, left axis) was noisy but almost instantaneous. The stress measurements were obtained by averaging over the last 50 s of each rate step, and supplemented by two values at $\dot{\gamma} = 100$ s^{-1}, measured just before and 50 s after the shear rate steps sequence. These five

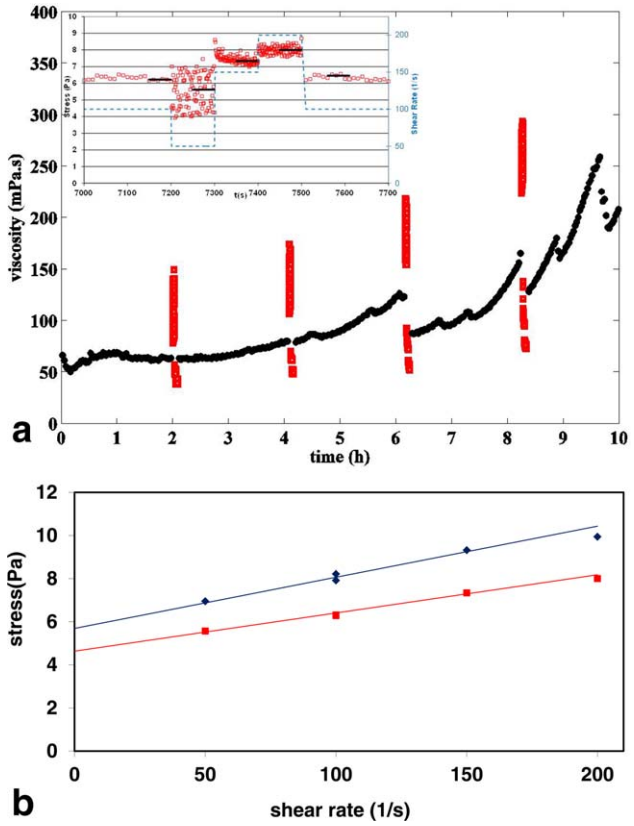

Figure 10. Top: Effective viscosity record, at $\dot{\gamma} = 100\ s^{-1}$ (black symbols) and response to shear rate steps (red open squares), of an olivine sample, at $\varphi = 20\%$, $T = 90°C$, $P_{CO_2} = 40$ bars. The inset displays the shear steps sequence (blue dotted line, right axis) applied at time $t = 2$ h, and the corresponding stress response (left axis, open red squares and black lines are the recorded values and their measurements, respectively). Bottom: Stress–strain values measured at times $t = 2$ h and $t = 4$ h (square and diamond symbols, respectively), compared with the corresponding Bingham plastic curves (straight lines). [Color figure can be viewed in the online issue, which is available at **wileyonlinelibrary.com**.]

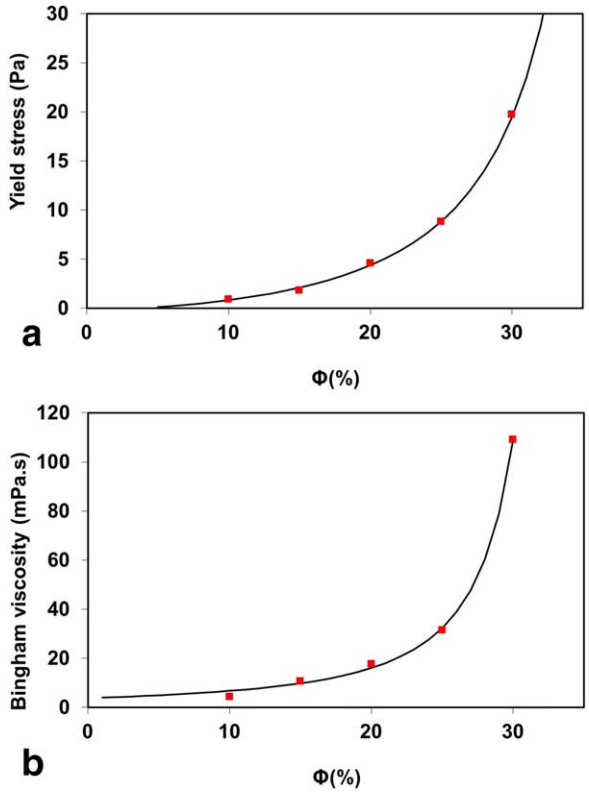

Figure 11. Yield stress (Σ_B, top) and Bingham viscosity (μ_B, bottom) measured on slurries, at different olivine concentrations, sheared 2 h at $\dot{\gamma} = 100\ s^{-1}$, $T = 90°C$, $P_{CO_2} = 40$ bars. The lines are fits to the data, using expressions (4) and (3) proposed by Wildemuth and Williams [8], for the yield stress and by Krieger and Dougherty [9], for the Bingham viscosity, respectively. [Color figure can be viewed in the online issue, which is available at **wileyonlinelibrary.com**.]

measurements are displayed in the stress–strain plot of Figure 10 (bottom panel), for the two aging times $t = 2$ h and $t = 4$ h. As expected, the initial and final values at $\dot{\gamma} = 100\ s^{-1}$ are comparable: There is no hysteresis. Moreover, the response is well described with a Bingham-plastic model of the form:

$$\Sigma = \Sigma_B + \mu_B \dot{\gamma} \tag{2}$$

where Σ_B is a yield stress and μ_B is the Bingham viscosity.

These quantities, measured for a volume fraction between $\varphi = 10\%$ and $\varphi = 30\%$, are displayed in Figure 11. The yield stress Σ_B increases with φ, from 1 to 20 Pa, which is in accordance with the above mentioned observation, that the pasty initial slurry does not flow from the vessel by its own weight at $\varphi > 30\%$. Such an order of magnitude (20 Pa at $\varphi = 30\%$) is also typical of slurries containing fine or ultrafine particles (particle size under 5 μm) [17–19], which are known to promote a yield stress. We note that in this kind of slurries, the rheology is not controlled solely by the hydrodynamic interactions, but depends also on Brownian interactions: Van der Walls, electrostatic. Thence, the rheology (and especially the yield stress) is expected to vary with the particle size distribution (which evolves with the dissolution/carbonation of the olivine), and with the temperature, pH, chemical composition of the dispersant [17–20], which leads to a rather complex slurry rheology, but also provides some monitoring tools.

DISCUSSION

First, our Bingham viscosity measurements can be fitted with a classical Krieger-Dougherty law [9] (see Figure 11, bottom),

$$\mu_B = \mu_o \left(1 - {}^{\varphi}/_{\varphi_{max}}\right)^{-n} \tag{3}$$

with $\mu_o = 3.8$ mPa s, $\varphi_{max} = 34.7\%$ and an exponent $n = 1.68$, in the range of the values reported in the literature (1.5 [21], 1.82 [9], 2 [22]). The values of μ_o and φ_{max} are more surprising. First, $\mu_o = 3.8$ mPa s is significantly higher than the value for the suspending water $\mu_{water} = 0.3$ mPa s at $T = 90°C$. Second, the value φ_{max}, which represents the packing fraction of the suspension, is unexpectedly small, compared to typical values 58% [23] or 60.5% [22] for suspensions of spheres [22,23]. We must stress however that in the present case, the system is more a gel than a suspension, as it has developed a yield stress. This yield stress compares very nicely to the analytical expression proposed by Wildemuth and Williams [8] (see Figure 11, top):

$$\Sigma_B = \sigma_o \left(\frac{\varphi/\varphi_o - 1}{1 - \varphi/\varphi_m} \right)^p \quad (4)$$

with $\sigma_o = 0.22$ Pa, $\varphi_o = 3.2\%$, $p = 0.79$, and φ_m (in line with the low value of φ_{max} found for the viscosity divergence). The so-obtained fitting values indicate that for an olivine volume fraction of about $\varphi_o = 3.2\%$, a yield stress of about $\sigma_o = 0.22$ Pa is expected to arise. We note that the "gel" transition value, $\varphi_o = 3.2\%$, is significantly higher than the values encountered in colloidal suspensions. Indeed, in the present case, the yield stress is expected to be promoted by the aggregation of the ultrafine (Brownian) particles [17,19], which only represent one part of the particles. Moreover, one expects some interplay between their aggregation and the aging conditions: The shear rate at $\dot{\gamma} = 100\ s^{-1}$ may promote the aggregation [24], whereas the shear stress may delay it though the breaking of the loose aggregates [8]. Moreover, the aggregates of ultrafine particles may sinter larger olivine particles which will then contribute to promote the yield stress.

The complexity of the system would require even more characterization in order to describe the complete scenario of the aging of the olivine suspension, during injection. In particular, the dissolution/precipitation reactions taking place in heterogeneous flows in fractures may be rather unexpected [3]. However, the trend plots characterizing the influence of olivine concentration, temperature, and CO_2 pressure, are encouraging: A significant time laps (several hours to 1 day or longer) exists before the thickening of the slurry, which should enable the slurry injection for sealing purposes. We note however that in the explored range of parameters, it is more likely that the stiffening of the slurry is controlled by the olivine dissolution [6], rather than by the carbonate precipitation [4]. In the case of a post injection sealing strategy, monitoring the delay of the olivine carbonation, in the various conditions encountered in the geological sites [25] is still an open challenging issue. However, with the prospect of a primitive well reinforcement process, the present Bingham characterization of the initial slurry gives the frame of a proper injection strategy [26–28].

ACKNOWLEDGMENTS

This work was supported by the COLINER project (ANR-08-PCO2-004) funded by the French National Research Agency (ANR). The authors thank A. Aubertin, L. Auffray and R. Pidoux for the design and the realization of the experimental set-up and acquisition procedure, Nuova Cives Srl for the olivine supply, and L. Talon and H. Auradou for stimulating discussions.

LITERATURE CITED

1. Bachu, S., & Bennion, D.B. (2009). Experimental assessment of brine and/or CO2 leakage through well cements at reservoir conditions, International Journal of Greenhouse Gas Control, 3, 494–501.
2. O'Connor, W.K., Dahlin, D.C., Nilsen, D.N., Walters, R.P., & Turner, P.C. (2000). Carbon dioxide sequestration by direct mineral carbonation with carbonic acid, Albany Research Center (ARC), Albany, OR.
3. Andreani, M., Luquot, L., Gouze, P., Godard, M., Hoise, E., & Gibert, B. (2009). Experimental study of carbon sequestration reactions controlled by the percolation of CO2-rich brine through peridotites, Environmental Science & Technology, 43, 1226–1231.
4. O'Connor, W.K., Dahlin, D.C., Rush, G.E., Gerdemann, S.J., Penner, L.R., & Nilsen, D.N. (2005). Aqueous mineral carbonation, Final Report, DOE/ARC-TR-04, 2.
5. Chen, Z.Y., O'Connor, W.K., & Gerdemann, S.J. (2006). Chemistry of aqueous mineral carbonation for carbon sequestration and explanation of experimental results, Environmental Progress, 25, 161–166.
6. Hänchen, M., Krevor, S., Mazzotti, M., & Lackner, K.S. (2007). Validation of a population balance model for olivine dissolution, Chemical Engineering Science, 62, 6412–6422.
7. Krevor, S.C.M., & Lackner, K.S. (2011). Enhancing serpentine dissolution kinetics for mineral carbon dioxide sequestration, International Journal of Greenhouse Gas Control, 5, 1073–1080.
8. Wildemuth, C.R., & Williams, M.C. (1984). Viscosity of suspensions modeled with a shear-dependent maximum packing fraction, Rheologica Acta, 23,627–635.
9. Krieger, I.M. (1972). Rheology of monodisperse latices, Advances in Colloid and Interface Science, 3, 111–136.
10. Leighton, D., & Acrivos, A. (1987). Shear-induced migration of particles in concentrated suspensions, Journal of Fluid Mechanics, 181, 415–439.
11. Deboeuf, A., Gauthier, G., Martin, J., Yurkovetsky, Y., & Morris, J.F. (2009). Particle Pressure in a Sheared Suspension: A Bridge from Osmosis to Granular Dilatancy, Physical Review Letters, 102, 108301-1–108301-4.
12. Quemada, D. (1977). Rheology of concentrated disperse systems and minimum energy dissipation principle, Rheologica Acta, 16, 82–94.
13. Jonckbloedt, R.C.L. (1998). Olivine dissolution in sulphuric acid at elevated temperatures—implications for the olivine process, an alternative waste acid neutralizing process, Journal of Geochemical Exploration, 62, 337–346.
14. Hänchen, M., Prigiobbe, V., Storti, G., Seward, T.M., & Mazzotti, M. (2006). Dissolution kinetics of fosteritic olivine at 90–150° C including effects of the presence of CO_2, Geochimica et cosmochimica acta, 70, 4403–4416.
15. Wogelius, R.A., & Walther, J.V. (1992). Olivine dissolution kinetics at near-surface conditions, Chemical Geology, 97, 101–112.
16. Pokrovsky, O.S., & Schott, J. (2000). Kinetics and mechanism of forsterite dissolution at 25°C and pH from 1 to 12, Geochimica et Cosmochimica Acta, 64, 3313–3325.
17. He, M., Wang, Y., & Forssberg, E. (2004). Slurry rheology in wet ultrafine grinding of industrial minerals: A review, Powder Technology, 147, 94–112.
18. Chun, J., Poloski, A.P., & Hansen, E.K. (2010). Stabilization and control of rheological properties of Fe_2O_3/Al $(OH)_3$-rich colloidal slurries under high ionic strength and pH, Journal of colloid and interface science, 348, 280–288.
19. Chun, J., Oh, T., Luna, M., & Schweiger, M. (2011). Effect of particle size distribution on slurry rheology: Nuclear waste simulant slurries, Colloids and Surfaces A: Physicochemical and Engineering Aspects, 384, 304–310.
20. Zhou, J.Z.Q., Uhlherr, P.H.T., & Luo, F.T. (1995). Yield stress and maximum packing fraction of concentrated suspensions, Rheologica Acta, 34, 544–561.
21. Ball, R.C., & Richmond, P. (1980). Dynamics of colloidal dispersions, Physics and Chemistry of Liquids, 9, 99–116.
22. Ovarlez, G., Bertrand, F., & Rodts, S. (2006). Local determination of the constitutive law of a dense suspension of noncolloidal particles through magnetic resonance imaging, Journal of Rheology, 50, p. 259.
23. Gauthier, G., Martin, J., & Salin, D. (2005). Gravity waves at the interface between miscible fluids and at the top of a settling suspension, Physical review letters, 94, 204501.
24. Guery, J., Bertrand, E., Rouzeau, C., Levitz, P., Weitz, D.A., & Bibette, J. (2006). Irreversible shear-activated aggregation in non-Brownian suspensions, Physical review letters, 96, 198301.

25. Wang, S., & Clarens, A.F. (2012). The effects of CO2-brine rheology on leakage processes in geologic carbon sequestration, Water Resources Research, 48, W08518.
26. Chen, M., Rossen, W., & Yortsos, Y.C. (2005). The flow and displacement in porous media of fluids with yield stress, Chemical Engineering Science, 60, 4183–4202.
27. Yun, M., Yu, B., Lu, J., & Zheng, W. (2010). Fractal analysis of Herschel–Bulkley fluid flow in porous media, International Journal of Heat and Mass Transfer, 53, 3570–3574.
28. Sochi, T. (2010). Modelling the flow of yield-stress fluids in porous media, Transport in Porous Media, 85, 489–503.